Computational and Theoretical Chemistry 1176 (2020) 112742

Contents lists available at ScienceDirect

Computational and Theoretical Chemistry

journal homepage: www.elsevier.com/locate/comptc

Quantum chemical and kinetic study of the $CCl_2 + HCl \rightarrow CHCl_3$ insertion reaction

Nicolás D. Gómez[a,*], M. Laura Azcárate[a], Jorge Codnia[a], Carlos J. Cobos[b]

[a] Departamento de Investigaciones en Láseres y Aplicaciones (CITEDEF- UNIDEF-CONICET), J.B. de La Salle 4397 (B1603ALO), Buenos Aires, Argentina
[b] Instituto de Investigaciones Fisicoquímicas Teóricas y Aplicadas (INIFTA), Departamento de Química, Facultad de Ciencias Exactas, Universidad Nacional de La Plata, CONICET, Casilla de Correo 16, Sucursal 4, La Plata (1900), Argentina

ARTICLE INFO

Keywords:
CCl_2
HCl
$CHCl_3$
Quantum-chemical calculations
Transition state theory
Halogenated radicals

ABSTRACT

The $CCl_2 + HCl \rightarrow CHCl_3$ (1) insertion reaction has been investigated by ab initio molecular orbital and kinetic calculations. The geometries of reactants, products and transition state were optimized with a large number of density functional theory (DFT) formulations combined with the 6-311++G(3*df*,3*pd*) basis set. The reaction barriers calculated with G4(MP2)//DFT and G4//DFT theories of 1.16 ± 0.27 and 0.61 ± 0.26 kcal mol^{-1} are consistent with the barrier height of $\Delta E_0^{\#} = 1.54 \pm 0.30$ kcal mol^{-1} estimated from the room temperature experimental rate constant. Calculated enthalpies of reaction of −53.97 ± 0.09 (G4(MP2)//DFT), −55.27 ± 0.09 (G4//DFT) and −56.52 ± 3.90 kcal mol^{-1} (DFT) agree well with experimental values. The obtained rate constants over the 300–2000 K temperature range at the high and low pressure limit can be expressed as $k_{1,\infty}$(G4(MP2)//DFT) = $(4.8 \pm 1.8) \times 10^{-14}$ $(T/300\,\mathrm{K})^{2.12 \pm 0.19}$ and $k_{1,\infty}$(G4//DFT) = $(9.8 \pm 3.4) \times 10^{-14}$ $(T/300\,\mathrm{K})^{1.77 \pm 0.16}$ in cm^3 molecule^{-1} s^{-1}, and $k_{1,0}$ = [HCl] 3.40×10^{-27} $(T/300\,\mathrm{K})^{-6.57}$ exp(−2218 K/*T*) cm^3 molecule^{-1} s^{-1}. Falloff curves for the intermediate pressure range obtained for the reactions (1, −1) with these rate constants and a derived central broadening factor of $F_{cent} = 0.16 + 0.84$ exp(−*T*/331 K) + exp(−7860 K/*T*) were compared with reported experimental rate data.

1. Introduction

Halogenated hydrocarbons such as chlorinated methanes and ethanes, vinyl chloride, polychlorinated biphenils (PCBs) and DDT (dichlorodiphenyltrichloroethylene), among others, constitute a family of hazardous wastes [1]. These types of compounds, have been frequently used as solvents in industrial areas because of their advantageous properties such as being non toxic and cheap. Organohalogens are very poorly biodegradable and, due to their strong chemical stability, energetic destruction processes are required. Particularly, chlorine containing radicals are obtained in the decomposition of chlorinated hydrocarbons [2] and are important intermediates in stratospheric chemistry. The destruction of halocarbons is more likely to form toxic halogenated by-products in the presence of O_2. The incineration of chlorocarbons may proceed through the elimination of a very reactive chlorine atom accelerating the process of decomposition [3]. The presence of chlorine also prevents the oxidation of CO to CO_2 and favours the production of harmful products such as dioxins, furans and phosgene. The thorough understanding of the chemical kinetic steps involved in chlorinated hydrocarbon combustion would contribute to utilize incineration in a more effective manner, to better assess the applicability and limitations of this process and to control the emission of toxic compounds. In addition, the manufacturing of chemicals by the controlled oxidation and pyrolysis of chlorinated hydrocarbons may be made possible through the detailed knowledge of their reaction pathways.

Since the development of high power lasers in the infrared and vacuum ultraviolet spectral ranges much research has been carried on in the field of laser decomposition of halogenated hydrocarbons and organohalogenes. UV photolysis and Infrared MultiPhoton Dissociation (IRMPD) have been extensively applied to the study of the fluorochlorocarbene radicals' kinetics. Photolytic methods have been successfully applied to generate radicals in the gas phase and allow the control of the degree of internal excitation of the fragments and, the combination of the photolysis with molecular beams allows for efficient cooling of the fragments.

In the last decades, development of organic and computational chemistry as well as of laser technology has enhanced interest in carbene chemistry. Halocarbenes are ideal systems for understanding the spectroscopy, photochemistry and photophysics of carbenes.

* Corresponding author.
E-mail addresses: ndgomez@citedef.gob.ar (N.D. Gómez), cobos@inifta.unlp.edu.ar (C.J. Cobos).

https://doi.org/10.1016/j.comptc.2020.112742
Received 3 December 2019; Received in revised form 16 January 2020; Accepted 3 February 2020
Available online 04 February 2020
2210-271X/

Dichlorocarbene, CCl_2, is one of the most typical carbenes. It undergoes direct insertion reactions into single bonds as well as addition to multiple bonds. These characteristics confer a high reactivity to this species. Its physical and chemical properties have been extensively studied. Most of the investigations have been focused on its spectrum.

The ground state singlet CCl_2 biradical is formed in the pyrolysis, combustion and photolysis of chlorinated hydrocarbons and is the main product in the thermal decomposition of $CHCl_3$ and CCl_2CO [4]. Hine et al. have also studied the formation of CCl_2 in the basic hydrolysis of $CHCl_3$ [5] and Huie et al. have obtained CCl_2 radicals through the O (^3P) + $CF_2CCl_2 \rightarrow F_2CO + CCl_2$ [6] reaction.

At present, the kinetics of this radical is an active area of research since it is a highly reactive intermediate. Especially, its reactivity with species such as O_x, HO_x, NO_x, FO_x and ClO_x (x = 0, 1, 2) is very important in atmospheric chemistry. Kinetic modeling of these processes is essential for understanding their mechanisms and the success of the models depends on having accurate information regarding the rate constants and the mechanisms of the reactions.

Previous studies of the kinetics of CCl_2 radicals with halogenated and unsaturated hydrocarbons as well as with simple molecules of atmospheric interest have been carried on by different authors. In 1980 Tiee et al. [7] determined the reaction rate constants of CCl_2 with NO, F_2, CO and C_3H_8 and reported an upper limit for the rate constants of the reactions with O_2 and C_2H_4. In 2000, Merelas et al. [8] measured the rate constants for the collisional removal of CCl_2 generated in the IRMPD of $CF_2 = CCl_2$ by simple alkenes and $CF_2 = CCl_2$ at room temperature. In 2003 Shestov et al. obtained CCl_2 radicals by photolysis of CCl_4 using a 193 nm excimer laser and studied its kinetics with Cl_2 and NO in the 300–750 K temperature range [9,10]. In 2004 Liu et al. [11,12] produced CCl_2 radicals by CCl_4 UV photolysis and determined the reaction rate constants with NO, C_2H_4, N_2O, CCl_4, $CHFCl_2$, CF_2Cl_2 and CH_2Cl_2 by time resolved laser induced fluorescence. They also determined the rate constant for the reactions with CH_2Cl_2 and C_2H_2 and proposed that they proceed through insertion and cycloaddition mechanisms. In 2008, using laser photolysis of CCl_4 and photoionization mass spectrometry, Eskola et al. [13] made the first direct measurements of the reaction rate constants of the CCl_2 radicals with Br_2 and NO_2 at temperatures between 266 and 365 K.

Regarding these previous works, discrepancies are found in the reported values of the rate constants of the reactions of CCl_2 with C_2H_4 and NO. On one hand, Tiee et al. have reported a rate constant of 3×10^{-13} cm^3 molecule^{-1} s^{-1} for the reaction with NO and an upper limit of 3×10^{-15} cm^3 molecule^{-1} s^{-1} for the reaction with C_2H_4 [7]. On the other, for the reaction with C_2H_4 values much higher than the one reported by Tiee have been obtained by other authors. Merelas et al. [8] reported a rate constant of 2.4×10^{-12} cm^3 molecule^{-1} s^{-1} while Liu et al. [11] obtained 3.5×10^{-13} cm^3 molecule^{-1} s^{-1}. For the CCl_2 + NO reaction, Liu et al. [11] obtained a rate constant value of 7.5×10^{-13} cm^3 molecule^{-1} s^{-1} which is almost a factor 2 higher than that measured by Tiee et al. [7]. The only experimental value of the rate constant of the reaction of CCl_2 with CO, 5×10^{-14} cm^3 molecule^{-1} s^{-1}, has been reported by Tiee et al. [7]. However, Shestov et al. calculated this parameter using transition state theory and obtained a significantly smaller value of 3.8×10^{-18} cm^3 molecule^{-1} s^{-1} [4].

Tetrachloroethylene, C_2Cl_4, is a widely used chlorinated solvent, and is one of the main products obtained in the self-recombination reaction between CCl_2 radicals and the knowledge of its kinetics is very important in understanding the impact in tropospheric chemistry. Kumaran et al. [14], Won et al. [15] and Zhu et al. [16] have studied the thermal decomposition of $CHCl_3$ and have reported values of the rate constant of the self-recombination reaction between CCl_2 radicals. Kumaran et al. studied the pyrolysis of 1% and 4% $CHCl_3$ diluted in Kr between 1282 and 1878 K. They used the laser-schlieren technique to measure $CHCl_3$ decomposition rate and followed Cl formation by time-resolved Cl atom resonance absorption. They set forth a kinetic reaction mechanism consisting of six elementary reactions to describe the secondary CCl_2 chemistry and reported the rate constant value of the self-recombination reaction in the low pressure regime. In 2003 Zhu et al. studied the thermal chlorination of $CHCl_3$ and proposed a mechanism of 38 reactions to explain the Cl_2 concentration decrease [16]. They characterized rate constants as functions of pressure and temperature using QRRK theory and performed master equation calculations for the analysis of stabilization effects. They reported $CHCl_3 \rightarrow CCl_2 + HCl$ to be the main channel for $CHCl_3$ decomposition and calculated the rate constant value of the self-recombination reaction at 0.1 atm pressure in the 300–2000 K temperature range. In other work, Won and Bozzelli studied the pyrolysis of 1% $CHCl_3$ diluted in 760 Torr of Ar in the 800–1073 K temperature range and determined the time and temperature dependence of the reactant and products formation by gas chromatography [15]. They proposed a detailed kinetic reaction mechanism consisting of 31 species and 67 elementary reactions to describe the loss of reactant and the formation of products and calculated the temperature dependence of the self-recombination reaction rate constant in a 760 Torr of Ar bath.

The reactions of intermediate products formed in the decomposition of chlorinated compounds with HCl are very important in atmospheric chemistry since significant quantities of HCl are generated from atmospheric reactions of Cl with diverse chlorinated methanes. For example, Won studied the thermal decomposition of C_2Cl_4 in excess of H_2 and found that Cl formed in the decomposition process reacts very efficiently with H_2 to form HCl with a high yield [2]. In reference [17] Schug et al. studied the thermal decomposition of $CHClF_2$, CHF_3 and $CHCl_3$ behind incident and reflected shock waves, reporting expressions for the low and high pressure limiting rate constants. No kinetic data was reported for the inverse recombination reactions. Bryukov et al. showed that HCl formation is the main mechanism in the reaction of Cl with CH_4, CH_3Cl, CH_2Cl_2 and $CHCl_3$ [18]. Knowledge of the kinetic parameters of the reactions of HCl with chlorocarbons is very important for understanding the efficiency of the UV decomposition of these compounds in the atmosphere as well as in their pyrolysis and combustion during the disposal of hazardous wastes. Especially, the reaction of CCl_2 with HCl significantly affects the $CHCl_3$ decomposition efficiency.

In our laboratory we have extensively studied the kinetics of the CCl_2 radical with a flash-photolysis facility with laser induced fluorescence (LIF) detection technique. In these studies CCl_2 radicals were obtained from the IRMPD of $CDCl_3$ in mixtures with Ar, O_2, HCl and NO_2 [19–27] and the products formed have been determined by Fourier Transform Spectrometry. In mixtures with Ar, C_2Cl_4 was observed as a major product while in mixtures with HCl we have also observed $CHCl_3$ as a major product. These products are associated to the $CCl_2 + CCl_2$ and CCl_2 + HCl reactions. In the experiments with NO_2 and O_2, CCl_2O was observed as one of the main products and its formation could be explained by the mechanisms: $CCl_2 + NO_2 \rightarrow CCl_2O + NO$ and $CCl_2 + O_2 \rightarrow CCl_2O + O$. These studies motivated a thorough search in the literature of information regarding the kinetic parameters of these reactions which led us to realize that kinetic information about CCl_2 reactivity was quite scarce.

The implemented LIF detection technique allowed to considerably simplify the reaction mechanism and to determine the $CDCl_3$ IRMPD probability [19] and the reaction rate constants of the CCl_2 radicals in a direct manner [28,29]. We have reported the first direct determination of the rate constant of the self-recombination reaction of CCl_2 radicals and of the association reaction between CCl_2 and HCl. The rate constant of the self recombination reaction determined in the high pressure limit was $k_\infty = (6.7 \pm 0.2) \times 10^{-13}$ cm^3 molecule^{-1} s^{-1}. The LIF technique was also used to determine the rate constant of the reaction between CCl_2 radicals and HCl [29]. The enthalpy of the CCl_2 + HCl $\rightarrow$ $CHCl_2$ + Cl reaction can be estimated in 18.9 kcal mol^{-1} [30] and, since the reaction CCl_2 + HCl + M $\rightarrow$ $CHCl_3$ + M (1) is exothermic in 56 kcal mol^{-1} [31], the first reaction was thus not included in the kinetic analysis. The determined rate constant for this process is k_1 =

$(2.7 \pm 0.1) \times 10^{-14}$ cm^3 $molecule^{-1}$ s^{-1} and no pressure dependence was observed for k_1 in the HCl 5–40 Torr pressure range.

Although halocarbenes such as CCl_2 have proven to be valuable benchmarks for comparing experiments with ab initio theory, few theoretical works about the reactivity of these radicals have been reported in the literature. In the works of Liu et al. the mechanism of the $CCl_2 + CH_2Cl_2$ [11], $CCl_2 + C_2H_2$ and $CCl_2 + H_2O$ [12] gas phase reactions were studied both experimentally and theoretically using high level ab initio theory, but no kinetic calculations have been performed. Pliego et al. [32] investigated the potential energy surface for the $H_2O + CCl_2$ reaction at the ab initio SCF and MP2 levels of theory employing DZP basis set in order to determine the mechanism of the basic aqueous decomposition of CCl_2. In 2004 Merrer et al. studied the reaction paths for addition of CCl_2 to 1,2-disubstituted cyclopropenes using hybrid density functional theory [33]. In 2007 Li et al. studied the mechanism, thermodynamics and kinetics of the CCl_2 insertion reaction into CH_2O using B3LYP optimized geometries and CCSD(T) single point energy calculations [34]. Shestov et al. studied the thermochemistry of the $CCl_2 + CO$ reaction using CCSD(T)/6-311 + G(3*df*)//CCSD/6-31G(*d*) level of theory and calculated the rate constant using transition state theory [4]. In a previous work we have theoretically studied the temperature and pressure dependence of the CCl_2 self-recombination reaction rate constant between 300 and 2000 K [35]. We employed quantum chemical calculations to characterize the potential energy along the reaction coordinate and determined the relevant molecular properties using density functional theory (DFT) [36] and ab initio methods. We have determined the high pressure rate constant by SSACM [37] and SACM/CT [38] calculations and the rate constant in the low pressure regime by the Troe's factorized formalism [39–40].

We have found limited information in the literature regarding reaction (1), and particularly, significant discrepancies are found in previous reports regarding the barrier height of reaction. In the study of the thermal decomposition of $CHCl_3$, Kumaran et al. [14] estimated a value of 3.8 kcal mol^{-1} for the back insertion barrier. Zhu et al. [16] calculated a value of 57 kcal mol^{-1} for the decomposition barrier of $CHCl_3$, and reported a barrier value of approximately 1 kcal mol^{-1} for the reverse insertion reaction. Herman et al. [41] estimated a reverse $CDCl_3$ decomposition barrier of 2.8–6.5 kcal mol^{-1}. The room temperature experimental rate constant value of reaction (1) suggests that the reaction proceeds through an electronic potential with a low energy barrier for the entrance association channel. Thus, this reaction is a useful benchmark for assessing the efficiency of different quantum-chemical models for determining its energetics.

In the present work, the kinetics of reaction (1) was studied using different DFT and ab initio quantum-chemical models to characterize their minimum energy path along the reaction coordinate, and unimolecular reaction rate theory was used to calculate the rate constant over wide pressure and temperature ranges. The results of the present work are very important to assess the discrepancies found in the literature regarding the thermochemistry of reaction (1), and for a complete understanding of its kinetics. The present work completes the information found in the literature regarding the CCl_2 radical kinetics and contributes to the development of kinetic models for application in the description of the combustion, pyrolysis and photolysis reactions of chlorinated hydrocarbons.

2. Theoretical methods

The canonical transition state theory (CTST) was employed in the determination of the rate constants of the $CCl_2 + HCl \rightarrow CHCl_3$ insertion reaction in the high pressure regime, $k_{1,\infty}$ [42]. The low pressure rate constants $k_{1,0}$ were obtained using the theory of thermal unimolecular reactions at low pressures developed by Troe [39,40]. The fall off curves were described by fully empirical representations of the RRKM theory that interpolates between the low and high pressure values [43]. The molecular properties of reactants, product and transition state were determined using the density functional theory (DFT) combined with the 6-311 + + G(3*df*,3*pd*) basis set. Regarding density functional methods, B3LYP is among the most widely used ones, yielding accurate predictions for many properties. In the present work, we have made a complete characterization of DFT theory performance in the calculation of the barrier height of the reaction. Diverse DFT formulations were employed. Becke three parameter hybrid functionals B3LYP [44], B3P86 [45] and B3PW91 [46–50] were used. Among one parameter hybrid functionals B1LYP [51–53], PBE1PBE [54,55], PBEh1PBE, mPW1PW91 and mPW1PBE [56] were also used. Among functionals including LYP correlation O3LYP [57] and X3LYP [58] were used. The long range corrected functionals LC-ωPBE [59–61], CAM-B3LYP [62] and wB97X-D [63] were employed. The hybrid functionals M06-2X [64], M05-2X and BMK [65] which include the Generalized Gradient Approximation (GGA) were also used. Other hybrid functionals employed were B97-1 [66], B98 [67], TPSSh [68], M06-HF [69], BH&HLYP [70], M06 [69] and mPW3PBE [56]. The double hybrid functionals B2PLYP [71] and mPW2PLYP [72] were also used. Among hybrid density functionals developed for thermochemical kinetics, in addition to the abovementioned M06-2X and BMK, the MPW1K [73], BB1K [74] and KMLYP [75] approaches were employed. The barrier heights and the reaction enthalpies were calculated with the G4 [76] and G4(MP2) [77] composite models. These approaches to the CCSD(T) theory provide average absolute deviations from the G3/05 test set of accurate thermochemical experimental data of 0.83 and 1.04 kcal mol^{-1}, respectively. All calculations were carried out with the Gaussian 09 package [78].

3. Results

3.1. Thermochemistry of the reaction

The geometries of the reactants, products and the transition state were optimized using the aforementioned DFT levels. The molecular structure of the transition state for the studied insertion reaction is shown in Fig. 1. The geometrical parameters along with the harmonic vibrational frequency assigned to the reaction coordinate are listed in Table 1. The configuration of the transition state is approximately planar with a mean r_{CH} value of 1.40 Å and a mean $\angle HCCl_c$ angle of 13.2. IRC calculation confirmed that the transition state links the reactants CCl_2 and HCl with the product $CHCl_3$.

The reaction proceeds *via* a three center HCl insertion. IRC calculation performed at the B3LYP/6-311 + + G(3*df*,3*pd*) level of theory shows that the reaction proceeds through the insertion of CCl_2 into the HCl bond almost as an association between the hydrogen atom of HCl and the carbon atom of CCl_2, without the formation of an association complex. The overall result is the insertion of the C into the HCl bond, implying the rupture of the HCl bond and the initial formation of the C—H bond, and subsequently the C-Cl bond is formed giving the $CHCl_3$ molecule. Calculations of the energetics of the reaction along the reaction coordinate are described in Fig. S1 of the Supplementary Material and an animation of the molecular geometry along the

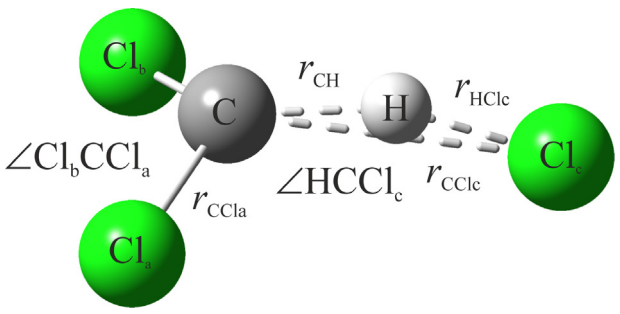

Fig. 1. Structure of the transition state for the $CCl_2 + HCl \rightarrow CHCl_3$ reaction.

Table 1
Geometrical parameters of the transition state for reaction $CCl_2 + HCl \rightarrow CHCl_3$. Bond lengths in Å, angles in degrees (see Fig. 1) and frequencies in cm^{-1}.

Level of theory	r_{CCla}	r_{CH}	r_{CClc}	r_{HClc}	$\angle Cl_bCCl_a$	$\angle HCCl_c$	$\angle Cl_aCHCl_c$	ν
B3LYP	1.69	1.42	2.84	1.47	114.5	11.1	73.8	491i
BMK	1.70	1.36	2.78	1.50	114.2	15.2	72.8	458i
M06-2X	1.67	1.31	2.72	1.55	115.6	19.1	74.0	633i
M05-2X	1.66	1.37	2.77	1.50	115.1	15.9	73.5	1097i
B2PLYP	1.68	1.38	2.80	1.48	114.8	12.9	74.7	602i
mPW2PLYP	1.67	1.37	2.79	1.49	115.0	13.4	73.7	643i
M06-HF	1.65	1.28	2.66	1.58	116.1	24.2	75.3	970i
X3LYP	1.68	1.42	2.84	1.47	114.5	11.2	74.2	496i
O3LYP	1.68	1.44	2.85	1.46	114.3	9.5	73.8	282i
PBE1PBE	1.67	1.43	2.83	1.45	114.4	11.4	73.6	254i
B97-1	1.69	1.44	2.84	1.46	113.9	11.5	72.9	282i
B98	1.69	1.42	2.83	1.46	114.0	11.6	73.0	298i
mPW1PW91	1.67	1.42	2.82	1.46	114.5	11.6	73.4	305i
PBEh1PBE	1.67	1.43	2.83	1.45	114.4	11.6	73.4	305i
B3P86	1.68	1.46	2.85	1.44	114.1	10.5	73.5	207i
BH&HLYP	1.66	1.31	2.78	1.54	116.2	13.8	76.6	803i
B3PW91	1.68	1.44	2.85	1.45	114.3	10.7	73.6	265i
mPW3PBE	1.68	1.46	2.85	1.44	114.1	10.5	73.5	215i
B1LYP	1.68	1.39	2.83	1.49	114.8	11.8	74.1	615i
LC-ωPBE	1.65	1.27	2.73	1.56	116.5	18.0	76.1	613i
CAM-B3LYP	1.66	1.34	2.79	1.52	115.7	14.0	75.3	637i
TPSSh	1.69	1.44	2.85	1.46	113.8	11.1	72.7	394i
M06	1.68	1.45	2.79	1.45	113.9	15.2	70.5	168i
mPW1PBE	1.67	1.42	2.83	1.46	114.4	11.5	73.6	276i
ωB97X-D	1.67	1.33	2.76	1.53	115.5	15.3	74.5	507i
MPW1K	1.67	1.34	2.78	1.51	116.0	13.5	76.3	548i
KMLYP	1.64	1.33	2.76	1.51	116.2	14.2	77.6	604i
BB1K	1.67	1.34	2.78	1.51	115.7	13.6	76.1	701i

reaction coordinate is given in the electronic material.

Barrier heights of the CCl_2 + HCl reaction were calculated with the DFT formalisms employed and the resulting DFT barrier heights are shown in Table 2. A summary of the barrier heights calculated with the different density functionals used is presented in the Supplementary Material, describing the calculated barrier heights adding Grimme's dispersion correction and long range correction in pure functionals, Table S1 and Table S2, respectively. In Table S3 of the Supplementary Material we also illustrate the calculated barrier heights using the M06-2X functional with different basis sets. Calculated energies for CCl_2, HCl, $CHCl_3$ and $CHCl_3^{\#}$ are listed in Table S4 of the Supplementary Material. As can be seen, the derived barrier heights for almost all the DFT formalisms are negative. Analysis of the barrier height calculations with the density functional theory has shown that the only functionals that produce positive values are BH&HLYP and M06-HF, giving 0.79 kcal mol^{-1} and 1.41 kcal mol^{-1}, respectively. The BH&HLYP hybrid functional has shown to predict transition state geometries and barrier heights reasonably well, despite being inferior to B3LYP for thermochemical properties, and the M06-HF functional has shown good overall performance in systems where the use of full Hartree-Fock exchange is important, to avoid the error of self interaction at long range. Especially, the geometry of the transition state obtained with the M06-HF functional differs significantly from those obtained with the other functionals. The r_{CH} length is significantly smaller than the ones obtained with other functionals with a value of 1.28 Å and the $HCCl_c$ angle is the highest with a value of 24.2 degrees. Also, the absolute values of the frequencies associated to the reaction coordinate, 970i cm^{-1} with M06-HF and 803i cm^{-1} with BH&HLYP are higher than the ones calculated with the other functionals except for the M05-2X functional for which a value of 1097i cm^{-1} is obtained.

Table 2
Barrier heights, $\Delta E_0^{\#}$, and reaction enthalpies, ΔH_0^{o}, (in kcal mol^{-1}) for $CCl_2 + HCl \rightarrow CHCl_3$ calculated with different DFT methods.

Level of theory	$\Delta E_0^{\#}$	ΔH_0^{o}	Level of theory	$\Delta E_0^{\#}$	ΔH_0^{o}
B3LYP	−2.93	−51.31	BH&HLYP	0.79	−55.14
BMK	−0.89	−58.25	B3PW91	−3.97	−54.72
M06-2X	−1.28	−58.63	mPW3PBE	−4.92	−56.15
M05-2X	−2.00	−60.14	B1LYP	−1.79	−51.00
B2PLYP	−2.61	−54.42	LC-ωPBE	−0.083	−61.62
mPW2PLYP	−2.70	−55.65	CAM-B3LYP	−1.67	−55.86
M06-HF	1.41	−65.88	TPSSh	−4.37	−53.50
X3LYP	−3.29	−52.30	M06	−2.78	−54.39
PBE1PBE	−5.05	−57.98	mPW1PBE	−4.39	−57.06
B97-1	−4.09	−54.24	B98	−3.68	−53.68
mPW1PW91	−4.28	−56.79	PBEh1PBE	−5.04	−57.72
B3P86	−5.15	−56.52	O3LYP	−1.78	−48.69
MPW1K	−3.79	−61.38	BB1K	−1.77	−58.49
KMLYP	−3.98	−64.91	ωB97X-D	−1.96	−56.05

In order to obtain a better value for $\Delta E_0^{\#}$, more accurate ab initio electronic structure calculations were carried out. First, we describe the calculations with the CCSD(T)/cc-pV*n*Z//B3LYP/6-311++G(*3df,3pd*) level of theory using the correlation consistent basis sets cc-pV*n*Z (where n = D, T and Q). The total electronic energies for the transition state (TS), CCl_2 and HCl as a function of basis set are shown in Fig. 2. An extrapolation with the function $E(n) = E_{CBS} + B \exp(-Cn)$ was used to approach the complete basis set limit. The results obtained (in Hartrees) for the different species are $E_{CBS}(TS) = -1417.845240$, $E_{CBS}(CCl_2) = -957.472212$ and $E_{CBS}(HCl) = -460.372885$. B3LYP/6-311++G(3*df*,3*pd*) zero-point energies (in Hartrees) are 0.011222, 0.004065 and 0.006707 for TS, CCl_2 and HCl, respectively. The calculated barrier heights with the different levels of theory are 2.48, 1.38 and 0.70 kcal mol^{-1} for n = D, T and Q, respectively. And, the resulting barrier height at the complete basis set limit, $\Delta E_0^{\#} = \Delta E_{CBS} + \Delta E_{ZP}$ (where $\Delta E_{CBS} = E_{CBS}(TS) - (E_{CBS}(CCl_2) + E_{CBS}(HCl))$ and $\Delta E_{ZP} = E_{ZP}(TS) - (E_{ZP}(CCl_2) + E_{ZP}(HCl))$), is 0.19 kcal mol^{-1}, showing better performance than DFT models. The results of the calculations of the electronic contribution to the barrier height are summarized in Table 3.

To ensure that the transition state of reaction (1) is well treated with a single reference based wavefunction, the T1 diagnostic of Lee and Taylor was employed [79,80]. The T1 diagnostic is often used as a qualitative estimate of the degree of multireference character of a system. For a closed shell species, a value of T1 = 0.02 has been suggested by Lee and Taylor as a threshold value. For considerably greater values, the reliability of single reference methods would become

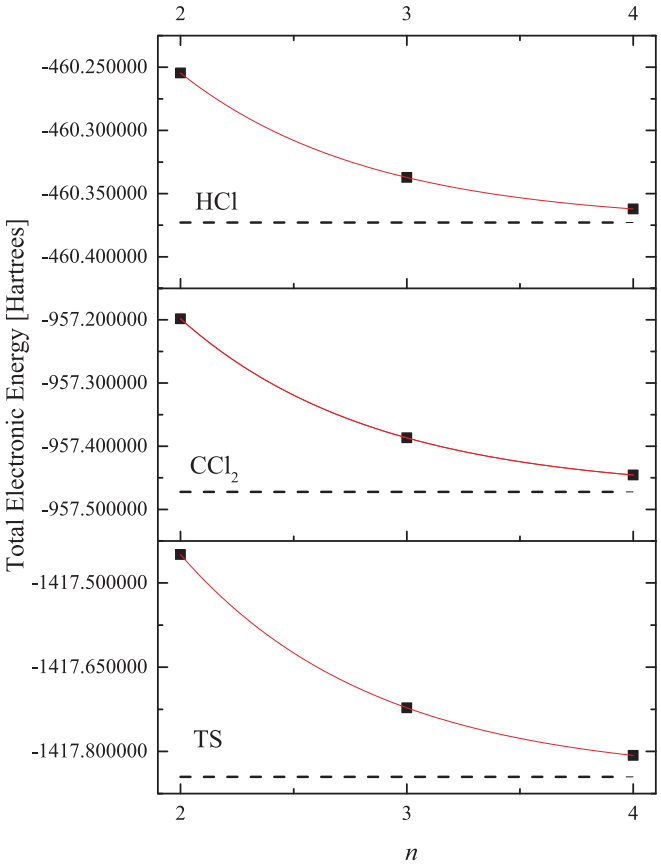

Fig. 2. Plots of total electronic energy (in Hartrees) for the transition state, CCl_2 and HCl as a function of the basis set size. The dotted lines indicate the extrapolated energy values.

questionable. As can be observed in Table 3, the computed T1 values of the transition state decrease as the quality of the basis set increases. Therefore, at the complete basis set limit, a T1 value lower than 0.02 could be surely expected, supporting the present CCSD(T) results.

Hence, according to the above considerations, we made single point energy calculations at the G4 and G4(MP2) levels using molecular structures obtained from the DFT calculations. The threshold energies and the reaction enthalpies at 0 K calculated with G4 and G4(MP2) levels of theory are listed in Table 4. Tables S5 and S6 of the Supplementary Material show the energies calculated for all the species with the G4//DFT/6-311++G(3*df*,3*pd*) and G4(MP2)//DFT/6-311++G(3*df*,3*pd*) levels of theory. It can be observed that the anomalous results obtained with the DFT theory are now corrected. The mean values of $\Delta E_0^{\#}$ calculated with the G4 and G4(MP2) levels of theory are 0.61 kcal mol^{-1} and 1.16 kcal mol^{-1}. Although these results are in good agreement within the theoretical error, the $\Delta E_0^{\#}$ obtained at the G4(MP2) level of theory is ~0.5 kcal mol^{-1} higher than the one obtained at the G4 level. Fig. S5 of the Supplementary Material illustrates the results of the barrier heights calculated with the different quantum-chemical models. As detailed in the Supplementary Material, lower values in the calculation of the barrier height with the G4 theory are due to calculations including fourth order perturbation theory.

A histogram of the $\Delta E_0^{\#}$ values derived from all employed methods is depicted in Fig. 3. Fig. 4 shows the mean values and the standard deviation of the $\Delta E_0^{\#}$ calculated with the different methods. The barrier height values calculated using DFT theory, DFT-D3 theory and DFT including the long range correction were −2.8 ± 1.8, −4.7 ± 1.5 and −2.7 ± 1.1 kcal mol^{-1}. In the Supplementary Material we present a review of the precision of different chemistry models regarding the calculation of chemical reaction barrier heights. From Fig. S4 of the

Table 4
Barrier heights and reaction enthalpies (in kcal mol^{-1}) calculated for $CCl_2 + HCl \rightarrow CHCl_3$ at 0 K with the G4 and G4(MP2) models. Single-point energy calculations were performed with molecular geometries optimized at the DFT level of theory with the 6-311++G(3*df*,3*pd*) basis set.

Level of theory		$\Delta E_0^{\#}$	ΔH_0^{o}
G4(MP2)	B3LYP	1.00	−53.89
	BMK	1.52	−53.76
	M06-2X	1.42	−53.96
	M05-2X	1.05	−53.98
	B2PLYP	1.16	−53.92
	mPW2PLYP	1.26	−53.90
	M06HF	0.84	−54.16
	X3LYP	1.01	−53.93
	PBE1PBE	1.10	−53.97
	B97-1	1.03	−53.97
	B98	1.13	−53.94
	mPW1PW91	1.14	−53.96
	PBEh1PBE	1.04	−53.97
	B3P86	0.85	−53.99
	BH&HLYP	1.85	−53.78
	B3PW91	0.96	−54.00
	mPW3PBE	0.91	−54.01
	B1LYP	1.20	−53.88
	LC-ωPBE	1.65	−54.03
	CAM-B3LYP	1.63	−53.96
	TPSSh	0.75	−54.05
	M06	1.17	−54.07
	mPW1PBE	1.15	−53.97
	APF	1.04	−53.99
G4	B3LYP	0.42	−55.20
	BMK	0.95	−55.13
	M06-2X	0.85	−55.25
	M05-2X	0.50	−55.25
	B2PLYP	0.61	−55.46
	mPW2PLYP	0.70	−55.18
	M06HF	0.32	−55.40
	X3LYP	0.47	−55.21
	PBE1PBE	0.55	−55.27
	B97-1	0.48	−55.28
	B98	0.58	−55.26
	mPW1PW91	0.59	−55.26
	PBEh1PBE	0.49	−55.28
	B3P86	0.31	−55.30
	BH&HLYP	1.25	−55.04
	B3PW91	0.42	−55.31
	mPW3PBE	0.37	−55.31
	B1LYP	0.65	−55.15
	LC-ωPBE	1.07	−55.28
	CAM-B3LYP	1.04	−55.22
	TPSSh	0.23	−55.37
	M06	0.66	−55.41
	mPW1PBE	0.60	−55.27
	APF	0.49	−55.29

Table 3
CCSD(T) total electronic energies (in Hartrees) for CCl_2, HCl and $CHCl_3^{\#}$. Barrier heights in kcal mol^{-1}. The calculated T1 values are indicated in parentheses.

Basis Set	CCl_2	HCl	$CHCl_3^{\#}$	$CCl_2 + HCl \rightarrow CHCl_3^{\#}$
cc-pVDZ	−957.198289	−460.254586	−1417.449371 (0.0203)	2.20
cc-pVTZ	−957.386775	−460.337209	−1417.722238 (0.0195)	1.10
cc-pVQZ	−957.445565	−460.362126	−1417.807021 (0.0190)	0.42
CBS limit	−957.472212	−460.372885	−1417.845240	−0.09

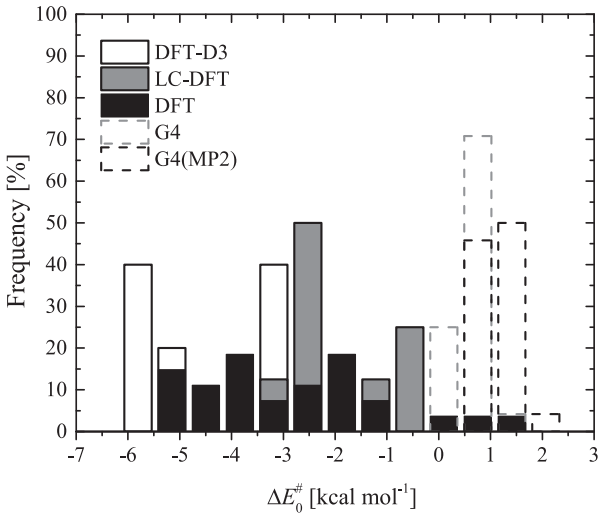

Fig. 3. Histogram of the $\Delta E_0{}^{\#}$ values calculated for $CCl_2 + HCl \rightarrow CHCl_3$ with the different levels of theory utilized.

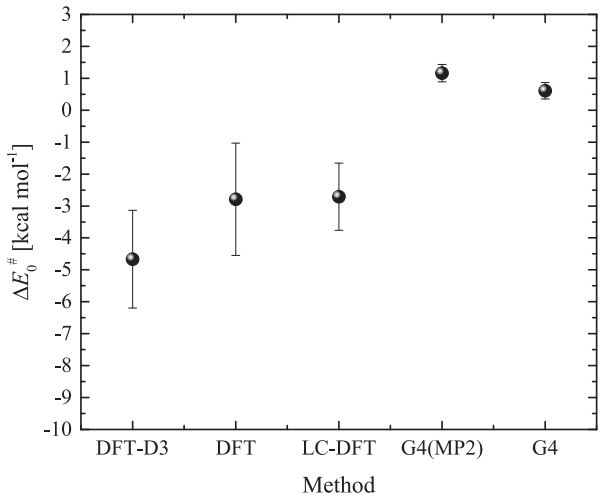

Fig. 4. Mean and standard deviation values of $\Delta E_0{}^{\#}$ calculated for $CCl_2 + HCl \rightarrow CHCl_3$ using different quantum chemical methods.

Supplementary Material we can observe that the precision attained by DFT methods has a similar magnitude to the barrier height calculated with the G4(MP2) and G4 chemistry models. The most precise DFT approach is the heavily parameterized hybrid meta-GGA M06-2X functional, yielding a mean unsigned error for the DBH24/08 database of 0.98 kcal mol^{-1} [81]. The rest of the functionals have mean unsigned errors ranging from 1.2 kcal mol^{-1} (BB1K) to 6.38 kcal mol^{-1} (TPSSh).

The methods with best performance are the G4(MP2) (MUE = 0.59 kcal mol^{-1}) and the G4 (MUE = 0.58 kcal mol^{-1}), resulting in barrier heights of 1.16 ± 0.27 and 0.61 ± 0.26 kcal mol^{-1}, respectively. It can also be observed that, within the theoretical error, the $\Delta E_0{}^{\#}$ value calculated with the CCSD(T)/CBS level of theory of 0.19 kcal mol^{-1} is in good agreement with those derived from the G4 and G4(MP2) calculations.

In Fig. 5 we illustrate the results adding dispersion and long range corrections to the pure models BLYP, BPW91 and PBEPBE. Barrier height values using single point energy calculations with the G4(MP2) and G4 theories are also shown. As can be observed DFT models including dispersion give the worst results. Addition of long range correction results in higher values of the barrier height, and the best performance is attained by G4(MP2) and G4 levels of theory. It can be as well observed that, although equivalent within theoretical error, the

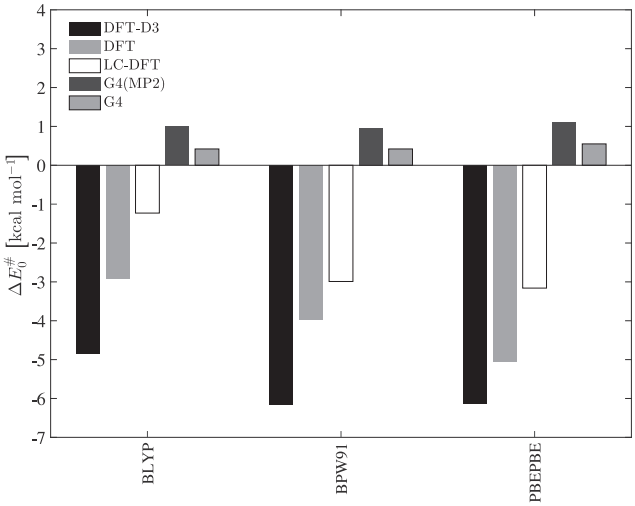

Fig. 5. $\Delta E_0{}^{\#}$ values calculated for $CCl_2 + HCl \rightarrow CHCl_3$ using different levels of theory. DFT-D3 corresponds to the hybrid DFT theory including D3 version of Grimme's dispersion [82]. DFT are the calculations with B3LYP, B3PW91 and PBE1PBE hybrid functionals. LC-DFT corresponds to the results of the calculations including long-range corrections. G4(MP2) and G4 are the calculated barrier heights using single point energy calculations at the employed optimized geometries.

calculations using the G4(MP2)//DFT/6-311 + + G(3*df*,3*pd*) level of theory are systematically higher than the ones obtained with the G4//DFT/6-311 + + G(3*df*,3*pd*) chemistry model.

The enthalpy of reaction calculated with the density functional theory was −56.52 ± 3.90 kcal mol^{-1}, while values of −53.97 ± 0.09 kcal mol^{-1} and −55.27 ± 0.09 kcal mol^{-1} were respectively obtained with the G4(MP2) and G4 theories. These results are comparable within theoretical error, even though G4(MP2) and G4 theories result in more precise values. The reaction enthalpy may be obtained from the measured enthalpies of the species of interest. Employing the NASA heats of formation at 0 K for the species HCl, CCl_2 and $CHCl_3$ of −22.02 ± 0.02, 54.6 ± 0.2 and −23.4 ± 0.6 kcal mol^{-1}, the value $\Delta H_0{}^{\circ}$ = −56.0 ± 0.6 kcal mol^{-1} is obtained. This value is in very good agreement with the values calculated in the present work. Table 5 summarizes the results.

The threshold energy for the reverse dissociation reaction (−1) is calculated as the sum of the enthalpy of the dissociation reaction and the energy barrier for the insertion process: $E_0 = \Delta H_0{}^{\circ} + \Delta E_0{}^{\#}$. From DFT, G4(MP2) and G4 calculations the threshold energy of the HCl elimination form $CHCl_3$ is determined to be 56.52, 55.13 and 55.88 kcal mol^{-1}. Kumaran et al. determined by RRKM calculations an E_0 value of 56 kcal mol^{-1} in good agreement with the thermochemical calculations of the present work. In other work, Herman et al. [41] estimated an enthalpy of $\Delta H_{300\ K}{}^{\circ}$ = 56 ± 3 kcal mol^{-1} for the dissociation reaction and measured the translation energy of the fragments produced in the IRMPD of $CDCl_3$. They performed RRKM calculations supposing that the fragments were rotationally and vibrationally cold, and obtained that the velocity distribution of the fragments was consistent with a reverse barrier in the 2.8–6.5 kcal mol^{-1} range. This value is significantly higher than the one calculated in the present work,

Table 5
$\Delta H_0{}^{\circ}$ values for the $CCl_2 + HCl \rightarrow CHCl_3$ reaction.

Method	$\Delta H_0{}^{\circ}$ [kcal mol^{-1}]
DFT	−56.52 ± 3.90
G4//DFT	−55.27 ± 0.09
G4(MP2)//DFT	−53.97 ± 0.09
Ref. 31	−56.0 ± 0.6

suggesting that the fragments might be rotationally and vibrationally excited in their experiments. The barrier height calculated in the present work is in good concordance with the estimation of Zhu et al., who calculated for the decomposition barrier a value of 57 kcal mol^{-1}, estimated for the enthalpy of reaction at 0 K a value of 56 kcal mol^{-1} and reported a barrier value of about 1 kcal mol^{-1} for the reverse insertion reaction [16].

The derived molecular properties described in the present Section were employed in the calculation of the rate constants of both the insertion and the reverse dissociation reaction. The Sections 3.2–3.4 will we focused on the estimation of the rate constants in the high and low pressure limits and in the intermediate fall-off range.

3.2. High pressure rate constant

The $CCl_2 + HCl \rightarrow CHCl_3$ reaction proceeds through a transition state located at the energy maximum along the reaction coordinate over the potential energy surface. Therefore, the high pressure recombination rate constant $k_{1,\infty}$ can be studied using the canonical version of the transition state theory (CTST) [42]

$$k_{1,\infty} = \frac{k_B T}{h} \frac{Q_{CHCl3^{\#}}}{Q_{CCl2} Q_{HCl}} e^{-\Delta E_0^{\#}/k_B T} \quad (1)$$

Here $Q_{CHCl3\#}$, Q_{CCl2} and Q_{HCl} are the total partition functions (electronic, translational, rotational and vibrational) of the transition state $CHCl_3^{\#}$, CCl_2 and HCl. The partition functions were calculated employing the DFT molecular parameters, and for the transition state barrier height we used the results obtained with the G4 and G4(MP2) calculations. The results obtained for $k_{1,\infty}$ at 300 K are listed in Tables 6 and 7.

The mean value of the high pressure rate constants calculated with the G4//DFT and G4(MP2)//DFT methods are $(1.4 \pm 0.6) \times 10^{-13}$ and $(5.1 \pm 2.3) \times 10^{-14}$ cm^3 molecule^{-1} s^{-1}, respectively. The pre-exponencial factor calculated as $A_\infty = k_B T/h\ Q_{CHCl3\#}/Q_{CCl2}Q_{HCl}$ at 300 K is $(3.6 \pm 1.7) \times 10^{-13}$ cm^3 molecule^{-1} s^{-1}. The unique experimental value reported for the insertion rate constant is the one obtained in our laboratory at room temperature and over the 5 to 40 Torr HCl pressure range: $k_{HCl} = (2.7 \pm 0.1) \times 10^{-14}$ cm^3 molecule^{-1} s^{-1} [29]. Using this experimental value and the above pre-exponential factor we found that the insertion reaction $CCl_2 + HCl$ proceeds with an energy barrier of $\Delta E_0{}^{\#} = 1.54 \pm 0.30$ kcal mol^{-1}, as illustrated in Fig. 6 and in good agreement, within theoretical error, with the values calculated using the G4(MP2) and G4 theories.

In Figs. S2 and S3 of the Supplementary Material we show that the performance of the models employed in the present work for the determination of the barrier height of the $CCl_2 + HCl$ reaction, are similar to the one observed in the calculation of the barrier heights of diverse reactions in the HTBH38/04 benchmark database [83].

Comparison of the experimental and calculated values of the rate constant show that the most exact values are those obtained by single point energy calculations with the G4(MP2) theory using geometries optimized at the BMK/6-311++G(3*df*,3*pd*) and M06-2X/6-311++G(3*df*,3*pd*) levels of theory. Regarding the performance of DFT theory for the determination of transition state geometries, Xu et al. used the TSG48 database to assess the performance of the Minnesota density functionals and 26 other high performance and popular density functionals for locating transition state geometries [84]. They concluded that most of the hybrid meta-GGAs combined with the MG3S basis set predict better transition state geometries than GGAs and hybrid GGAs, M06-2X and BMK were found among the meta-GGAs with better performance and the widely used B3LYP hybrid functional was found to have a poor performance. The values of the rate constant calculated in the present work with the G4//M06-2X/6-311++G(3*df*,3*pd*) and G4//BMK/6-311++G(3*df*,3*pd*) combined models are also in very good agreement with the experimental result. The predicted temperature dependence for $k_{1,\infty}$ between 300 and 2000 K is

$$k_{1,\infty} = (4.8 \pm 1.8)x10^{-14}(T/300\ K)^{2.12\pm0.19} cm^3\ molecule^{-1}s^{-1} \quad (G4(MP2)//DFT) \quad (2)$$

$$k_{1,\infty} = (9.8 \pm 3.4)x10^{-14}(T/300\ K)^{1.77\pm0.16} cm^3 molecule^{-1}s^{-1} \quad (G4//DFT) \quad (3)$$

Uncertainties correspond to ± 1 σ (Table S8 of the Supplementary Material).

3.3. Low pressure rate constant

At the low pressure limit the recombination reaction is determined by the intermolecular energy transfer. Therefore, the efficiency of the molecular collisions must be taken into account for the calculation of the low pressure rate coefficient, k_0. This parameter was determined by Troe's factorized formalism: $k_0 = \beta_c k_0^{sc}$ [39,40]. The strong collision recombination rate constant, k_0^{sc}, is characterized by the equilibrium population of molecular states and by the collision efficiency, β_c, which account for intermolecular energy transfer processes. The expressions for k_0^{sc} and β_c are given by Eqs. (4) and (5)

$$k_0^{sc} = \left(1/K_c\right)[M] Z_{LJ} \frac{\rho_{vib}(E_0) k_B T}{Q_{vib}} \exp\left(-\frac{E_0}{k_B T}\right) F_{anh} F_E F_{rot} F_{rotint} \quad (4)$$

$$-\langle \Delta E \rangle \approx F_E k_B T \frac{\beta_c}{1 - \sqrt{\beta_c}} \quad (5)$$

Here Z_{LJ} is the Lennard-Jones collision frequency between the formed excited adduct and the collider bath gas M, $E_0 = \Delta H_0{}^{o} + \Delta E_0{}^{\#}$ is the threshold dissociation energy at 0 K, $\rho_{vib,h}(E_0)$ is the harmonic vibrational density of states evaluated at E_0, F_E is a correction factor that accounts for the energy dependence of $\rho_{vib,h}(E_0)$, F_{anh} takes into account

Table 6
High pressure limit rate constants calculated for $CCl_2 + HCl \rightarrow CHCl_3$ at 300 K using the G4(MP2)//DFT level of theory. Employed barrier heights and enthalpies are listed in Table 4.

Level of theory	$k_{1,\infty}$ [cm^3 molecule^{-1} s^{-1}]	Level of theory	$k_{1,\infty}$ [cm^3 molecule^{-1} s^{-1}]
G4(MP2)//B3LYP	6.91×10^{-14}	G4(MP2)//PBEh1PBE	6.26×10^{-14}
G4(MP2)//BMK	2.25×10^{-14}	G4(MP2)//B3P86	8.29×10^{-14}
G4(MP2)//M06-2X	2.57×10^{-14}	G4(MP2)//BH&HLYP	1.84×10^{-14}
G4(MP2)//M05-2X	8.71×10^{-14}	G4(MP2)//B3PW91	6.77×10^{-14}
G4(MP2)//B2PLYP	5.19×10^{-14}	G4(MP2)//mPW3PBE	7.33×10^{-14}
G4(MP2)//mPW2PLYP	4.45×10^{-14}	G4(MP2)//B1LYP	4.99×10^{-14}
G4(MP2)//M06HF	1.01×10^{-13}	G4(MP2)//LC-ωPBE	2.11×10^{-14}
G4(MP2)//X3LYP	6.84×10^{-14}	G4(MP2)//CAM-B3LYP	2.43×10^{-14}
G4(MP2)//PBE1PBE	5.30×10^{-14}	G4(MP2)//TPSSh	9.93×10^{-14}
G4(MP2)//B97-1	5.70×10^{-14}	G4(MP2)//M06	4.14×10^{-14}
G4(MP2)//B98	4.74×10^{-14}	G4(MP2)//mPW1PBE	4.82×10^{-14}
G4(MP2)//mPW1PW91	5.01×10^{-14}	G4(MP2)//APF	5.88×10^{-14}

Table 7
High pressure limit rate constants calculated for $CCl_2 + HCl \rightarrow CHCl_3$ at 300 K using the G4//DFT level of theory. Employed barrier heights and enthalpies are listed in Table 4.

Level of theory	$k_{1,\infty}$ [cm^3 molecule^{-1} s^{-1}]	Level of theory	$k_{1,\infty}$ [cm^3 molecule^{-1} s^{-1}]
G4//B3LYP	1.82×10^{-13}	G4//PBEh1PBE	1.57×10^{-13}
G4//BMK	5.93×10^{-14}	G4//B3P86	2.05×10^{-13}
G4//M06-2X	6.67×10^{-14}	G4//BH&HLYP	5.03×10^{-14}
G4//M05-2X	2.18×10^{-13}	G4//B3PW91	1.67×10^{-13}
G4//B2PLYP	1.30×10^{-13}	G4//mPW3PBE	1.81×10^{-13}
G4//mPW2PLYP	1.13×10^{-13}	G4//B1LYP	1.25×10^{-13}
G4//M06HF	2.41×10^{-13}	G4//LC-ωPBE	5.57×10^{-14}
G4//X3LYP	1.69×10^{-13}	G4//CAM-B3LYP	6.53×10^{-14}
G4//PBE1PBE	1.33×10^{-13}	G4//TPSSh	2.37×10^{-13}
G4//B97-1	1.43×10^{-13}	G4//M06	9.71×10^{-14}
G4//B98	1.19×10^{-13}	G4//mPW1PBE	1.21×10^{-13}
G4//mPW1PW91	1.26×10^{-13}	G4//APF	1.48×10^{-13}

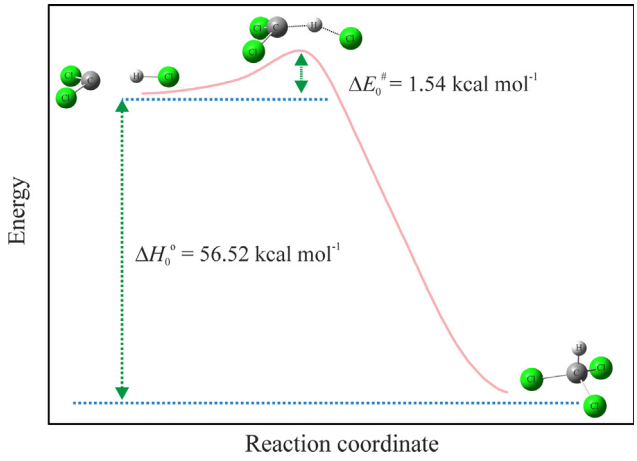

Fig. 6. Reaction scheme for $CCl_2 + HCl \rightarrow CHCl_3$. ΔH_0^{o} is the reaction enthalpy and $\Delta E_0^{\#}$ the activation energy barrier.

the vibrational anharmonicity, F_{rot} accounts for the rotational contributions to the threshold energy and the vibrational density of states and F_{rotint} describes the internal rotor behavior (taken as 1 for the present reaction), Q_{vib} is the vibrational partition function of the formed adduct, -⟨ΔE⟩ is the mean energy transferred by the collisions between the vibrationally excited $CHCl_3$ and the buffer gas M and K_c is the equilibrium constant evaluated from the total molecular partition functions, as determined in Eq. (6). -⟨ΔE⟩ is calculated with Eq. (7), as a function of the mean energy transferred in deactivating collisions, ⟨ΔE_{down}⟩, considered independent of temperature.

$$K_c = \frac{Q_{CCl2} Q_{HCl}}{Q_{CHCl3}} \exp\left(-\frac{\Delta H_0^o}{RT}\right) \quad (6)$$

$$\langle \Delta E \rangle = -\frac{\langle \Delta E_{down} \rangle^2}{\langle \Delta E_{down} \rangle + F_E k_B T} \quad (7)$$

Z_{LJ} was calculated using the Lennard-Jones parameters ε_{HCl}/k_B = 360 K, σ_{HCl} = 3.305 Å, ε_{CHCl3}/k_B = 327 K and σ_{CHCl3} = 5.43 Å [85]. The value $\rho_{vib,h}(E_0) = 1.94 \times 10^7$ (kcal mol^{-1})$^{-1}$ was calculated using the Whitten-Rabinovitch [86] approximation and for a reaction with a barrier, the value F_{anh} = 1 was employed. F_{rot} was calculated assuming the case I potential of Waage and Rabinovitch [87], using the ratio of moments of inertia $I^+/I = (I_B{}^+ I_C{}^+)/(I_B I_C) = 1.72$, $\Delta H_0{}^o$ = 56.52 kcal mol^{-1} as determined with the DFT level of theory and $\Delta E_0{}^{\#}$ = 1.54 kcal mol^{-1}, as determined with the calculations of the present work and the experimental rate constant [29]. We assumed a temperature independent ⟨ΔE_{down}⟩ value of 787 cm^{-1}, as reported by Kumaran et al. for Kr in their study of the thermal decomposition of $CHCl_3$. This value was taken in the present work as a representative value of the mean energy transferred in the collision between $CHCl_3$ and usual buffer gases as Kr, Ar, N_2 and He [88]. The frequencies of the vibrational modes and the $CHCl_3$ rotational constants were obtained with the B3LYP/6-311 + + G(3*df*,3*pd*) level of theory. The derived frequencies in cm^{-1} were, 259 (CCl_3 d-deform), 365 (CCl_3 s-deform), 667 (CCl_3 s-stretch), 732 (CCl_3 d-stretch), 1242 (CH bend), and 3188 (CH stretch). The calculated rotational constants were A = 0.11, B = 0.11 and C = 0.056 cm^{-1}. The values for the transition state vibrational frequencies are 65, 142, 345, 641, 768, 848, 1050 and 1062 cm^{-1}. The rotational constants of the transition state are A = 0.12, B = 0.055 and C = 0.038 cm^{-1}. The temperature dependence of the factors in Eqs. (4) and (5) are listed in Table 8. The derived expressions for $k_{1,0}$ and K_c over the 300–2000 K range are

$$k_{1,0} = [HCl]\ 3.40 \times 10^{-27} (T/300\ K)^{-6.57} exp(-2218\ K/T)\ cm^3\ molecule^{-1}\ s^{-1} \quad (8)$$

$$K_c = 1.18 \times 10^{28} (T/300\ K)^{-1.61} exp(-29,478\ K/T)\ molecule\ cm^{-3} \quad (9)$$

In Section 3.4 we describe the analysis of the pressure dependence of the rate coefficient of the insertion and the reverse dissociation reaction using a parameterized model, that interpolates the rate constant values between the previously determined low and high pressure rate coefficients. A comparison with previous reported data of the dissociation rate constant will be given. And, in particular, previous report of the insertion rate constant in reference [29] will be analyzed in terms of the calculations of the present work.

Table 8
Contributing factors to $k_{1,0}$ for reaction $CCl_2 + HCl + M \rightarrow CHCl_3 + M$. Z_{LJ} and $k_{1,0}$ in cm^3 molecule^{-1} s^{-1}, and K_c in molecule cm^{-3}. M = HCl.

T [K]	Z_{LJ}	Q_{vib}	F_E	F_{rot}	β_c	$k_{1,0}$	K_c
300	4.74×10^{-10}	2.65	1.07	5.84	0.61	2.58×10^{-30}	2.82×10^{-15}
1000	5.81×10^{-10}	1.39×10^{2}	1.29	2.89	0.22	1.41×10^{-31}	2.74×10^{14}
1250	6.12×10^{-10}	4.42×10^{2}	1.39	2.48	0.16	5.16×10^{-32}	6.99×10^{16}
1500	6.40×10^{-10}	1.24×10^{3}	1.49	2.18	0.12	2.05×10^{-32}	2.62×10^{18}
1750	6.66×10^{-10}	3.16×10^{3}	1.61	1.94	0.09	8.74×10^{-33}	3.31×10^{19}
2000	6.90×10^{-10}	7.37×10^{3}	1.75	1.76	0.06	3.96×10^{-33}	2.13×10^{20}

3.4. Rate constant in the falloff range

The rate constants in the intermediate pressure range were derived by interpolation between the limiting rate constants $k_{1,0}$ and $k_{1,\infty}$ employing the reduced expression

$$\frac{k}{k_{1,\infty}} = F_{LH}(x)F(x) \tag{10}$$

with $x = k_{1,0}/k_{1,\infty}$ [42]. The factor $F_{LH}(x) = x/(1+x)$ is the result of the simple Lindemann-Hinshelwood mechanism. The broadening factor $F(x)$ accounts for the multistep character of the energy transfer process assisted by collisions. Different expressions have been proposed for this factor and Eqs. (11)–(13) reproduce very well the asymmetric broadening factors for broad falloff curves, characterized by values of the center broadening factors, $F_{cent} = F(x = 1)$, lower than 0.4. Other proposed expressions for $F(x)$ perform equally well for $F_{cent} > 0.4$ [42].

$$F(x) = \frac{1+x}{[1+x^n]^{1/n}} \tag{11}$$

with

$$n = \left[\frac{ln(2)}{ln(2/F_{cent})}\right][1 - 0.15\,(1-x^q)] \tag{12}$$

$$q = (F_{cent} - 1)\,/ln(F_{cent}/10) \tag{13}$$

The essential magnitude in the broadening factor is the center broadening factor, F_{cent}. This can be expressed as $F_{cent} = F_{cent}^{WC} F_{cent}^{SC}$, where $F_{cent}^{WC} = \beta_c^{0.14}$ is the weak collision center broadening factor and F_{cent}^{SC} the strong collision center broadening factor [89,90] calculated with Eq. (14)

$$F_{cent}^{sc} = 10^{-\frac{(1.06log_{10}(s_k))^{2.2}}{1+C_1 s_k^{C_2}}} \tag{14}$$

Here C_1 and C_2 are given by Eqs. (15) and (16)

$$C_1 = 0.1\,exp(2.5\,b_k{}^{-1} - 0.22\,b_k - 6 \times 10^{-10} b_k{}^6) \tag{15}$$

$$C_2 = 1.9 + 4.6 \times 10^{-5} b_k{}^{2.8} \tag{16}$$

where s_k and b_k are the modified Kassel parameters, defined as $s_k = 1 + \frac{U_{vib}^{\#}}{k_B T}$ and $b_k = \left(\frac{s_k - 1}{s - 1}\right)^{1.6}\left(\frac{E_0 + a(E_0)E_z}{k_B T}\right)$, s being the number of vibrational modes of $CHCl_3$. Here $U_{vib}{}^{\#}$ is the transition state vibrational energy and $a(E_0)$ the Whitten-Rabinovitch correction factor. The parameters s_k and b_k were calculated using the above molecular parameters of $CHCl_3$. The results of the calculations are shown in Table 9 together with the calculated F_{cent} parameters.

The derived F_{cent} values are very well reproduced between 300 and 2000 K by the expression

$$F_{cent} = 0.16 + 0.84\,exp(-T/331\,K) + exp(-7860\,K/T) \tag{17}$$

In what follows, we compare the results of the present work with those previously reported. Temperature and pressure dependence of the rate constant were calculated using the above F_{cent}, $k_{1,0}$ and $k_{1,\infty}$ values. In Fig. 7 we depict the $k_{-1,\infty}$ values calculated for the $CHCl_3$

Table 9
Modified Kassel parameters and central broadening factor for reaction $CCl_2 + HCl \rightarrow CHCl_3$.

T [K]	s_k	b_k	F_{cent}^{WC}	F_{cent}^{SC}	F_{cent}
300	3.31	15.51	0.93	0.55	0.51
1000	6.14	16.76	0.81	0.25	0.20
1250	6.61	15.41	0.77	0.24	0.18
1500	6.94	14.10	0.74	0.24	0.18
1750	7.20	12.93	0.71	0.25	0.18
2000	7.40	11.91	0.68	0.26	0.18

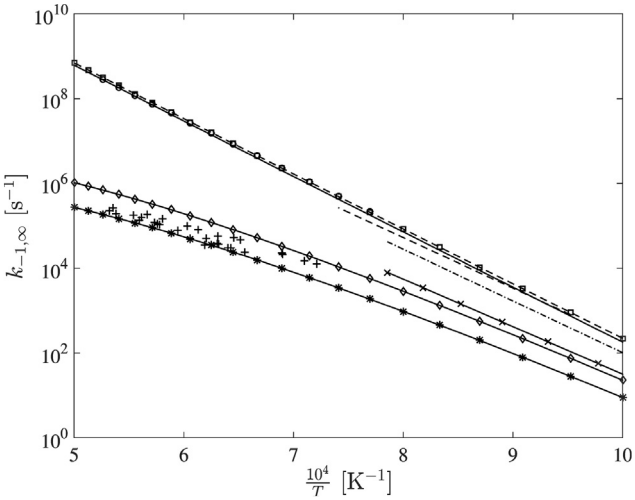

Fig. 7. Arrhenius plots for $k_{-1,\infty}$ —: This work. ——: Schug et al. [17]. -·-·-: Won et al. [15]. ○: Kumaran et al. [14]. -□-□-: Zhu et al. [16]. +: Kumaran et al. at ρ = 9.4 × 10^{17} molecules cm^{-3} [14]. -x-x-: Won et al. at 1 atm pressure of Ar [15]. -*-*-: This work at Kr = 9.4 × 10^{17} molecules cm^{-3} and using $\langle\Delta E_{down}\rangle$ = 787 cm^{-1}. -◊-◊-: This work at 1 atm and using $\langle\Delta E_{down}\rangle$ = 787 cm^{-1}.

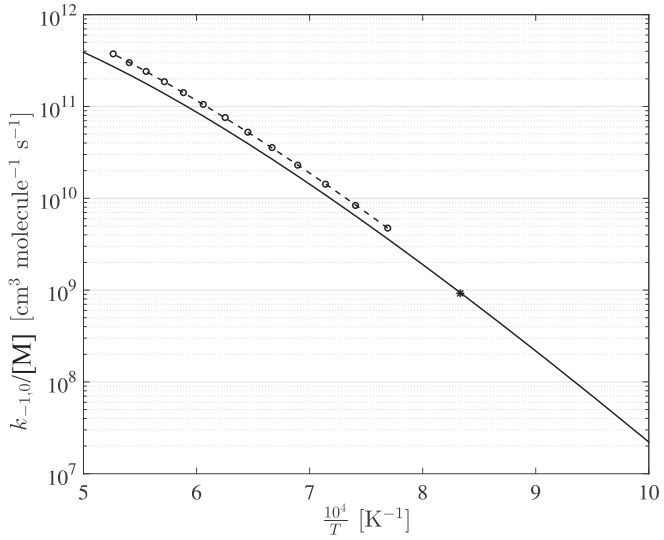

Fig. 8. Arrhenius plots for $k_{-1,0}$/[M]. —: This work for M = Kr and using $\langle\Delta E_{down}\rangle$ = 787 cm^{-1}, as determined by Kumaran et al. [14]. —: Troe's formalism from Kumaran et al. [14]. o: RRKM formalism from Kumaran et al. *: Schug et al. [17].

decomposition reaction and those reported by Kumaran et al. [14], Won et al. [15], Zhu et al. [16] and Schug et al. [17]. Also, in Fig. 8 we compare the calculated $k_{-1,0}$ with previous reported values.

Kumaran et al. calculated the rate of $CHCl_3$ dissociation using RRKM theory and Troe's semiempirical formalism considering Kr as buffer in the 1300–1900 K temperature range [14]. Their results were consistent with their own experimental results provided that E_0 = 56 kcal mol^{-1}, similar to our G4(MP2) and G4 values. The resulting RRKM rate constant log ($k_{-1,\infty}$/s^{-1}) = 15.21–58.97 (kcal mol^{-1})/(2.303RT) leads to the value 4.37 × 10^6 s^{-1} at 1500 K which is in good agreement with those obtained using the Eqs. (2) and (9), (2.3–5.2) × 10^6, and (3) and (9), (2.9–5.9) × 10^6 s^{-1}. Using the model of the present work in the calculation of $k_{-1,\infty}$ with $\Delta E_0{}^{\#}$ = 1.54 kcal mol^{-1} as estimated from the experimental rate constant [29], and $\Delta H_0{}^{o}$ = 56.52 kcal mol^{-1}, as determined with the DFT models, would give $k_{-1,\infty}$ = 3.6 × 10^6 s^{-1} at 1500 K, which is also in very good agreement with the result of

Kumaran et al. [14]. In Fig. 7 we can observe a very good agreement between the $k_{-1,\infty}$ values calculated at 1000–2000 K and those from Kumaran et al. [14]. We also illustrate the experimental results of Kumaran et al. for a concentration of $\rho = 10^{18}$ molecules cm^{-3} between 1300 and 1900 K, observing a very good agreement with the present results obtained for M = Kr and a $\langle\Delta E_{down}\rangle$ parameter as reported in reference [14]. We can also observe that our results are a factor 1.7 smaller than those reported by Won et al. [15].

For the low pressure dissociation rate constant Kumaran et al. reported $k_{-1,0}/[Kr] = 9.34 \times 10^{27}\ T^{-9.92}\ \exp(-33{,}480\ K/T)\ cm^3$ molecule^{-1} s^{-1} using an older Troe's formalism and $2.51 \times 10^{26}\ T^{-9.50}\ \exp(-32{,}536\ K/T)\ cm^3$ molecule^{-1} s^{-1} with the RRKM method [14]. The results of our calculations using Kr as buffer gas over the 1000–2000 K range are illustrated in Fig. 8, observing a very good agreement with the results obtained by Kumaran et al. These equations led to the values 5.89×10^{-14} and 6.41×10^{-14} cm^3 molecule^{-1} s^{-1} at 1500 K. Using Eqs. (8) and (9) of the present work we obtain 5.12×10^{-14} cm^3 molecule^{-1} s^{-1}, in very good agreement with the results of Kumaran et al. [14].

Zhu et al. [16] studied the thermal decomposition reaction of $CHCl_3$ in the presence of Cl_2 and determined from QRRK calculations the rate constant for the dissociation reaction. The rate expression in the high pressure regime determined using calculations at the G3//B3LYP/6-311G(d,p) level is $9.09 \times 10^{11}\ T^{0.941}\ \exp(-57.1\ kcal\ mol^{-1}/RT)\ s^{-1}$. The results of the calculations at 1000–2000 K are illustrated in Fig. 7, observing a very good agreement with the present work. Their values at 1000, 1500, and 2000 K of 2.1×10^2, 4.5×10^6 and 6.9×10^8 s^{-1} are in very good agreement with the results of our calculations using $\Delta E_0^{\#} = 1.54$ kcal mol^{-1} and $\Delta H_0^{o} = 56.52$ kcal mol^{-1}, 1.4×10^2, 3.6×10^6, 6.2×10^8 s^{-1}, respectively. The rate constant reported by Zhu et al. at 0.1 atm and using $\langle\Delta E_{down}\rangle = 1000\ cm^{-1}$ is $5.84 \times 10^{40} \times T^{-8.7}\ \exp(-63.9\ kcal\ mol^{-1}/RT)\ s^{-1}$. The calculated rate coefficient at 1000 K using Zhu et al. expression [16] is $5.4\ s^{-1}$, which is in excellent agreement with the result of the calculation using the model of the present work $6.3\ s^{-1}$, with the $\langle\Delta E_{down}\rangle$ employed by Zhu et al.

Won et al. calculated the $CHCl_3$ dissociation rate constant as a function of pressure and temperature [15]. They reported Arrhenius expressions for the rate constants in the high pressure limit of $1.6 \times 10^{14}\ \exp(-56\ kcal\ mol^{-1}/RT)\ s^{-1}$ and $5.2 \times 10^{12}\ \exp(-51.5\ kcal\ mol^{-1}/RT)\ s^{-1}$ for 1 atm Ar pressure. Evaluation of these expressions in the temperature range of their experiments is illustrated in Fig. 7. It can be observe that similar results are obtained using the expressions for $k_{-1,\infty}$, $k_{-1,0}$ and F_{cent} derived in the present work. For example, utilizing the rate expressions of Won et al. work we obtain at 1000 K the values $k_{-1,\infty} = 1.1 \times 10^2\ s^{-1}$ and $k_{-1}(1\ atm) = 34\ s^{-1}$. Using Eqs. (2) and (9) we obtain $k_{-1,\infty} = 1.7 \times 10^2\ s^{-1}$ and using Eqs. (3) and (9) $k_{-1,\infty} = 2.2 \times 10^2\ s^{-1}$ in good agreement with the values obtained with Won et al. expressions [15]. The result of the calculation using the above "experimental" $\Delta E_0^{\#} = 1.54$ kcal mol^{-1} value and $\Delta H_0^{o} = 56.52$ kcal mol^{-1} is $1.38 \times 10^2\ s^{-1}$, in better agreement with the result of Won et al. [15]. The rate constant obtained at 1 atm of Ar using the model of the present work with $\langle\Delta E\rangle_{down} = 787\ cm^{-1}$ [14] is $k_{-1}(1\ atm) = 19\ s^{-1}$, in very good agreement with the value reported by Won et al. [15].

In their study of the thermal decomposition of the $CHClF_2$, CHF_3 and $CHCl_3$ compounds behind incident and reflected shock waves, Schug et al. determined the temperature dependence of the high and low pressure limit rate constants [17] between 1050 and 1380 K. The data derived from the expression $k_{-1,\infty} = 1.8 \times 10^{14}\ \exp(-(55 \pm 3)$ kcal mol$^{-1}/RT)$ s^{-1} and the single rate constant $k_{-1,0}/[Ar] = 9.3 \times 10^8\ cm^3\ mol^{-1}\ s^{-1}$ determined at the mean temperature of the experiments, 1200 K, are depicted in Figs. 7 and 8. Both sets of results exactly match if, as before, the values $\Delta E_0^{\#} = 1.54$ kcal mol^{-1} and $\Delta H_0^{o} = 56.52$ kcal mol^{-1} are employed. Using Eqs. (8) and (9) of the present work we estimate $k_{-1,0}/[M](1200\ K) = 9.7 \times 10^8\ cm^3$ mol^{-1} s^{-1} in very good agreement with the value reported by Schug et al. [17].

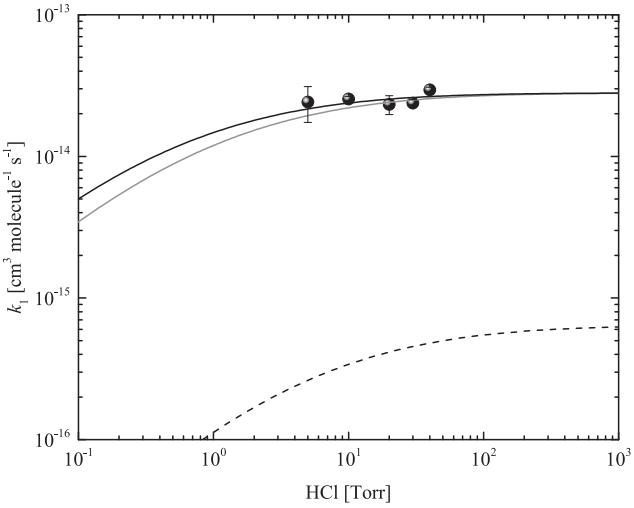

Fig. 9. Falloff curves for reaction $CCl_2 + HCl \rightarrow CHCl_3$ at 300 K. ●: Experimental rate constants from Ref. 28. gray line: Calculated with $\Delta H_0^{o} = 56.52$ kcal mol^{-1}, $\Delta E_0^{\#} = 1.54$ kcal mol^{-1}, $\langle\Delta E_{down}\rangle = 787\ cm^{-1}$, and $F_{anh} = 1$. black line: Calculated with $\Delta H_0^{o} = 56.52$ kcal mol^{-1}, $\Delta E_0^{\#} = 1.54$ kcal mol^{-1}, $\langle\Delta E_{down}\rangle = 787\ cm^{-1}$, and $F_{anh} = 1.79$ (see text). ———: Calculated with $\Delta H_0^{o} = 52.2$ kcal mol^{-1}, $\Delta E_0^{\#} = 3.8$ kcal mol^{-1} and $\langle\Delta E_{down}\rangle = 787\ cm^{-1}$ (Kumaran et al. [14]).

Regarding reaction (1), Fig. 9 shows the experimental rate constants measured over the 5–40 Torr range of HCl [29] and the calculated falloff curves at 300 K. The collision efficiency parameter β_c was calculated using $\langle\Delta E_{down}\rangle = 787\ cm^{-1}$, as determined for Kr by Kumaran et al. [14]. In Fig. 9 it can be observed that the rate constants derived from the present modeling with $\Delta E_0^{\#} = 1.54$ kcal mol^{-1} are in very good agreement with the experimental rate data. A better agreement could be obtained if an anharmonicity correction factor [39] in Eq. (4) of $F_{anh} = 1.79$ is employed. Although this treatment is strictly valid for a combination of Morse (barrierless) type oscillator with harmonic oscillators, all above results indicate that reaction (1) proceeds via a small height barrier located over a very flat potential surface. Therefore, the model of Ref. 39 could be assumed approximately valid for the present case. The resulting falloff curve is depicted in Fig. 9.

Also, in Fig. 9 we depicted the calculated rate constants using the formalism of the present work and the thermodynamic parameters as estimated by Kumaran et al., $\Delta H_0^{o} = 52.2$ kcal mol^{-1} and $\Delta E_0^{\#} = 3.8$ kcal mol^{-1} [14]. It can be observed that rate constants significantly underestimate the experimental values. Hence, the experimental results of Ref. 29 confirm that the reaction is very close to the high pressure limit and exhibit a recombination energy barrier about a factor of two smaller than the one reported by Kumaran et al. [14].

4. Conclusion

The $CCl_2 + HCl \rightarrow CHCl_3$ insertion reaction has been studied over the 300–2000 K temperature range. Molecular structures and harmonic vibrational frequencies for the transition state and all species were estimated using several DFT formalisms with the 6-311++G(3*df*,3*pd*) basis set. The energetics was determined by single-point calculations employing the G4(MP2)//DFT and G4//DFT models. The calculated mean reaction enthalpies and reaction barrier heights at 0 K are -53.97 ± 0.09 kcal mol^{-1} and 1.16 ± 0.27 kcal mol^{-1} at the G4(MP2)//DFT level, and -55.27 ± 0.09 kcal mol^{-1} and 0.61 ± 0.26 kcal mol^{-1} at the G4//DFT level. The ΔH_0^{o} value calculated with the DFT models is -56.52 ± 3.90 kcal mol^{-1}, in good agreement with those derived at the G4(MP2) and G4 levels of theory.

The threshold energies for the reverse dissociation process are -55.13 ± 0.36 and -55.88 ± 0.35 kcal mol^{-1}. These values are in good agreement with those reported by Kumaran et al. [14], Won et al. [15], Zhu et al. [16] and Schug et al. [17]. The calculated low pressure rate constant can be expressed as $k_{1,0} = [\mathrm{HCl}]\ 3.40 \times 10^{-27}\ (T/300\ \mathrm{K})^{-6.57}\ \exp(-2218\ \mathrm{K}/T)$ cm^3 molecule^{-1} s^{-1}. The determined high pressure rate constants at the G4(MP2)//DFT and G4//DFT levels are $k_{1,\infty} = (4.8 \pm 1.8) \times 10^{-14}\ (T/300\ \mathrm{K})^{2.12 \pm 0.19}$ and $k_{1,\infty} = (9.8 \pm 3.4) \times 10^{-14}\ (T/300\ \mathrm{K})^{1.77 \pm 0.16}$ cm^3 molecule^{-1} s^{-1}. The experimental room temperature rate constant measured in the falloff regime [29] is consistent with these limiting rate constants. The modeling with a broadening factor of $F_{\mathrm{cent}} = 0.16 + 0.84\ \exp(-T/331\ \mathrm{K}) + \exp(-7860\ \mathrm{K}/T)$ suggests that the reaction barrier at 0 K is about 1.5 kcal mol^{-1}.

CRediT authorship contribution statement

Nicolás D. Gómez: Conceptualization, Software, Formal analysis, Investigation, Writing - original draft, Visualization. **M. Laura Azcárate:** Project administration, Investigation, Supervision, Writing - review & editing. **Jorge Codnia:** Conceptualization, Validation, Writing - review & editing. **Carlos J. Cobos:** Supervision, Resources, Investigation, Formal analysis, Writing - review & editing, Visualization.

Declaration of Competing Interest

The authors declare that they have no known competing financial interests or personal relationships that could have appeared to influence the work reported in this paper.

Acknowledgments

This research project was supported by the Instituto de Investigaciones Científicas y Técnicas para la Defensa, the Universidad Nacional de La Plata (X842) and the Consejo Nacional de Investigaciones Científicas y Técnicas CONICET (PIP 2012-0134).

Appendix A. Supplementary material

Supplementary data to this article can be found online at https://doi.org/10.1016/j.comptc.2020.112742. These data include MOL files and InChiKeys of the most important compounds described in this article.

References

[1] G. Kamgang-Youbi, K. Poizot, F. Lemont, Inductively coupled plasma torch efficiency at atmospheric pressure for organo-chlorine liquid waste removal: chloroform destruction in oxidative conditions, J. Hazard. Mater. 244–245 (2013) 171–179.
[2] S.H. Kable, S.A. Reid, T.J. Sears, The halocarbenes: model systems for understanding the spectroscopy, dynamics and chemistry of carbenes, Int. Rev. Phys. Chem. 28 (3) (2009) 435–480.
[3] Y. Won, Thermal decomposition of tetrachloroethylene with excess hydrogen, J. Ind. Eng. Chem. 15 (2009) 510–515.
[4] A.A. Shestov, S.A. Kostina, V.D. Knyazev, Thermal decomposition of dichloroketene and its reaction with H atoms, Proc. Combust. Inst. 30 (2005) 975–983.
[5] J. Hine, Carbon dichloride as an intermediate in the basic hydrolisis of chloroform. A mechanism for substitution reactions at a saturated carbon atom, J. Am. Chem. Soc. 72 (6) (1950) 2438–2445.
[6] R.E. Huie, N.J.T. Long, B.A. Thrush, Laser induced fluorescence of CFCl and CCl_2 in the gas phase, Chem. Phys. Lett. 51 (1977) 197–200.
[7] J.J. Tiee, F.B. Wampler, W.W. Rice Jr., Reactions of CCl, CCl_2 and CClF radicals, Chem. Phys. Lett. 73 (1980) 519–521.
[8] I. Merelas, J.A. Fernández, P. Puyuelo, M.N. Sánchez Rayo, D. Husain, F. Castaño, The collisional removal of the carbene $CCl_2(\tilde{X}(0, 0, 0))$ and $CCl_2(\tilde{A}^1B_1(0, 7, 0))$ by rare gases and simple molecules, Chem. Phys. 254 (2000) 77–88.
[9] S.A. Kostina, A.A. Shestov, V.D. Knyazev, Kinetics of the reaction of the CCl2 biradical with molecular chlorine, J. Phys. Chem. A 107 (2003) 10292–10295.
[10] A.A. Shestov, S.A. Kostina, E.V. Shafir, I.R. Slagle, V.D. Knyazev, Kinetics of the reaction of the CCl_2 biradical with NO, Chem. Phys. Lett. 381 (5–6) (2003) 766–770.
[11] Y. Liu, Y. Xin, L. Pei, Y. Chen, Reaction kinetic studies of CCl_2 $(\tilde{X}(0, 0, 0))$ with several simple molecules, C. Chen, Chem. Phys. Lett. 385 (2004) 314–318.
[12] Y. Liu, Z. Zhang, L. Pei, Y. Chen, C. Chen, Reaction kinetic studies of CCl_2 $(\tilde{X}(0, 0, 0))$ with C_2H_2 and H_2O molecules, Chem. Phys. 303 (2004) 255–263.
[13] A.J. Eskola, I. Golonka, M.P. Rissanan, R.S. Timonen, Kinetics of the CCl_2 + Br 2 and CC_l2 + N_O2 reactions in the temperature range 266–365 K and reactivity of the CC_l2 biradical, Chem. Phys. Lett. 460 (2008) 401–405.
[14] S.S. Kumaran, M.C. Su, K.P. Lim, J.V. Michael, S. Klippenstein, J. DiFelice, P.S. Mudipalli, J.H. Kiefer, D.A. Dixon, K.A. Peterson, Experiments and theory on the thermal decomposition of $CHCl_3$ and the reactions of CCl_2, J. Phys. Chem. A 101 (1997) 8653–8661.
[15] Y.S. Won, J.W. Bozzelli, Chloroform pyrolysis: experiment and detailed reaction model, Combust Sci. Technol. 85 (1992) 345–373.
[16] L. Zhu, J.W. Bozzelli, Kinetics and mechanism for the thermal chlorination of chloroform in the gas phase: Inclusion of HCl elimination from $CHCl_3$, Int. J. Chem. Kinet. 35 (2003) 647–660.
[17] K.P. Schug, H. Gg, Wagner, F. Zable, Gas phase α, α elimination of hydrogen halides from halomethanes. I. Thermal decomposition of chlorodifluoromethane, trifluoromethane, and trichloromethane behind shock waves, Ber. Bunsenges. Phys. Chem. 83 (1979) 167–175.
[18] M.G. Bryukov, I.R. Slagle, V.D. Knyazev, Kinetics of reactions of Cl atoms with methane and chlorinated methanes, J. Phys. Chem. A 106 (2002) 10532–10542.
[19] N.D. Gómez, V. D'Accurso, J. Codnia, F.A. Manzano, M.L. Azcárate, Direct determination of the dissociation probability in highly focused IR multiple photon dissociation, App. Phys. B 106 (2012) 921–926.
[20] M.L. Azcárate, V.M. Freytes, J. Codnia, Intracavity system design for IR multiphoton dissociation, App. Phys. B 103 (2011) 687–693.
[21] V.M. Freytes, J. Codnia, M.L. Azcárate, Chloroform infrared multiphoton dissociation in the presence of O_2 and NO_2, Photochem. Photobiol. 81 (2007) 789–792.
[22] M.L. Azcárate, E.J. Quel, Infrared multiple-photon dissociation of $CDCl_3$ induced by a TEA CO_2 laser, Appl. Phys. B. 47 (1988) 239–242.
[23] M.L. Azcárate, E.J. Quel, Fluence and wavelenght dependence of the IRMPA and IRMPD of $CDCl_3$ with a CO_2 laser, Appl. Phys. B 47 (1988) 223–228.
[24] V.M. Freytes, J. Codnia, M.L. Azcárate, Láseres: Desarrollos y aplicaciones, Colección Ciencia y Tecnología, UNSAMedita, 2007.
[25] M.L. Azcárate, E.J. Quel, Isotopic selectivity and collisional deactivation in the infrared multiple-photon dissociation of $CDCl_3$ in equimolar $CDCl_3$/$CHCl_3$ mixtures, J. Phys. Chem. 93 (1989) 697–702.
[26] M.L. Azcárate, E.J. Quel, B. Toselli, J.C. Ferrero, E.H. Staricco, Collisional effects in the multiphoton absorption processes of $CDCl_3$, J. Phys. Chem. 92 (2) (1988) 403–408.
[27] C.A. Rinaldi, J.C. Ferrero, M.A. Vázquez, M.L. Azcárate, E.J. Quel, Collisional deactivation of $CDCl_3$ excited with a TEA CO_2 laser, J. Phys. Chem. 100 (1996) 9745–9750.
[28] N.D. Gómez, V. D'Accurso, V.M. Freytes, F.A. Manzano, J. Codnia, M.L. Azcárate, Kinetic study of the CCl_2 radical recombination reaction by laser-induced fluorescence technique, Int. J. Chem. Kin. 45 (2013) 306–313.
[29] N.D. Gómez, V. D'Accurso, F.A. Manzano, J. Codnia, M.L. Azcárate, Determination of the rate constant of the reaction of CCl_2 with HCl, Int. J. Chem. Kinet. 46 (2014) 382–388.
[30] NIST Standard Reference Database 13, http://kinetics.nist.gov/janaf/janaf4pdf.html, 1998.
[31] J.B. Burkholder, J.P.D. Abbatt, R.E. Huie, M.J. Kurylo, D.M. Wilmouth, S.P. Sander, J.R. Barker, C.E. Kolb, V.L. Orkin, P.H. Wine, Chemical Kinetics and Photochemical Data for Use in Atmospheric Studies, Evaluation Number 18, 2015. https://jpldataeval.jpl.nasa.gov/pdf/JPL_Publication_15-10.pdf.
[32] J.R. Pliego, Jr. De Almeida, W.B. De Almeida, Reaction Paths for Aqueous Decomposition of CCl2, J. Phys. Chem. 100 (1996) 12410–12413.
[33] D.C. Merrer, P.R. Rablen, Dichlorocarbene addition to cyclopropenes: a computational study, J. Org. Chem. 70 (2005) 1630–1635.
[34] Z.F. Li, L.L. Lu, J.W. Kang, Theoretical study on the mechanism and characters of thermodynamics and kinetics of the insertion reaction of CCl_2 into CH_2O, Acta Chim. Sin. 65 (2007) 1019–1026.
[35] N.D. Gómez, J. Codnia, M.L. Azcárate, C.J. Cobos, Quantum chemical and kinetic study of the CCl_2 self-recombination reaction, Comp. Theor. Chem. 1121 (2017) 1–10.
[36] K.J. Laidler, M.C. King, The development of transition-state theory, J. Phys. Chem. 87 (1983) 2657–2664.
[37] J. Troe, Theory of thermal unimolecular reactions at high pressures, J. Chem. Phys. 75 (1) (1981) 226–237.
[38] A.I. Maergoiz, E.E. Nikitin, J. Troe, V.G. Ushakov, Classical trajectory and statistical adiabatic channel study of the dynamics of capture and unimolecular bond fission. V. Valence interactions between two linear rotors, J. Chem. Phys. 108 (4) (1998) 9987–9998.
[39] J. Troe, Theory of thermal unimolecular reactions at low pressures. II. Strong collision rate constants, Appl. J. Chem. Phys. 66 (1977) 4758–4775.
[40] J. Troe, Theory of thermal unimolecular reactions at low pressures I. Solutions of the master equation, J. Chem. Phys. 66 (1977) 4745–4757.
[41] I.P. Herman, F. Magnotta, R.J. Buss, Y.T. Lee, Infrared laser multiplephoton dissociation of $CDCl_3$ in a molecular beam, J. Chem. Phys. 79 (1983) 1789–1794.
[42] S. Glasstone, K.J. Laidler, H. Eyring, The Theory of Rate Processes: The Kinetics of Chemical Reactions, Viscosity, Diffusion and Electrochemical Phenomena, McGraw-Hill Book Company Inc., New York, 1941, pp. 1–27.
[43] J. Troe, V.G. Ushakov, Representation of broad fall-off curves for dissociation and

recombination reactions, Z. Phys. Chem. 228 (2013) 1–10.
[44] A.D. Becke, Density-functional thermochemistry. III. The role of exact exchange, J. Chem. Phys. 98 (1993) 5648–5652.
[45] J.P. Perdew, Density-functional approximation for the correlation energy of the inhomogeneous electron gas, Phys. Rev. B 33 (1986) 8822–8824.
[46] J.P. Perdew, Electronic Structure of Solids '91, Ed. P. Ziesche and H. Eschrig, Akademie Verlag, Berlin, 1991.
[47] J.P. Perdew, J.A. Chevary, S.H. Vosko, K.A. Jackson, M.R. Pederson, D.J. Singh, C. Fiolhais, Atoms, molecules, solids, and surfaces: applications of the generalized gradient approximation for exchange and correlation, Phys. Rev. B 46 (1992) 6671–6687.
[48] J.P. Perdew, J.A. Chevary, S.H. Vosko, K.A. Jackson, M.R. Pederson, D.J. Singh, C. Fiolhais, Erratum: atoms, molecules, solids, and surfaces - applications of the generalized gradient approximation for exchange and correlation, Phys. Rev. B 48 (1993) 4978.
[49] J.P. Perdew, K. Burke, Y. Wang, Generalized gradient approximation for the exchange-correlation hole of a many-electron system, Phys. Rev. B 54 (1996) 16533–16539.
[50] K. Burke, J.P. Perdew, Y. Wang, Electronic Density Functional Theory: Recent Progress and New Directions, Ed. J. F. Dobson, G. Vignale and M. P. Das, Plenum, 1998.
[51] A.D. Becke, Density-functional exchange-energy approximation with correct asymptotic-behavior, Phys. Rev. A 38 (1988) 3098–30100.
[52] C. Lee, W. Yang, R.G. Parr, Development of the Colle-Salvetti correlation-energy formula into a functional of the electron density, Phys. Rev. B 37 (1988) 785–789.
[53] B. Miehlich, A. Savin, H. Stoll, H. Preuss, Results obtained with the correlation-energy density functionals of Becke and Lee, Yang and Parr, Chem. Phys. Lett. 157 (1989) 200–206.
[54] J.P. Perdew, K. Burke, M. Ernzerhof, Generalized gradient approximation made simple, Phys. Rev. Lett. 77 (1996) 3865–3868.
[55] J.P. Perdew, K. Burke, M. Ernzerhof, Errata: generalized gradient approximation made simple, Phys. Rev. Lett. 78 (1997) 1396.
[56] C. Adamo, V. Barone, Exchange functionals with improved long-range behavior and adiabatic connection methods without adjustable parameters: the mPW and mPW1PW models, J. Chem. Phys. 108 (1998) 664–675.
[57] A.J. Cohen, N.C. Handy, Dynamic correlation, Mol. Phys. 99 (2001) 607–615.
[58] F. Weigend, F. Furche, R. Ahlrichs, Gaussian basis sets of quadruple zeta valence quality for atoms H-Kr, J. Chem. Phys. 119 (2003) 12753–12762.
[59] O.A. Vydrov, G.E. Scuseria, Assessment of a long range corrected hybrid functional, J. Chem. Phys. 125 (2006) 234109.
[60] O.A. Vydrov, J. Heyd, A. Krukau, G.E. Scuseria, Importance of short-range versus long-range Hartree-Fock exchange for the performance of hybrid density functionals, J. Chem. Phys. 125 (2006) 074106.
[61] O.A. Vydrov, G.E. Scuseria, J.P. Perdew, Tests of functionals for systems with fractional electron number, J. Chem. Phys. 126 (2007) 154109.
[62] T. Yanai, D. Tew, N. Handy, A new hybrid exchange-correlation functional using the Coulomb-attenuating method (CAM-B3LYP), Chem. Phys. Lett. 393 (2004) 51–57.
[63] J.D. Chai, M.H. Gordon, Long-range corrected hybrid density functionals with damped atom-atom dispersions corrections, Phys. Chem. Chem. Phys. 10 (2008) 6615–6620.
[64] Y. Zhao, D.G. Truhlar, Comparative DFT study of van der Waals complexes: Rare-gas dimers, alkaline-earth dimers, zinc dimer, and zinc-rare-gas dimers, J. Phys. Chem. 110 (2006) 5121–5129.
[65] A.D. Boese, J.M.L. Martin, Development of Density Functionals for Thermochemical Kinetics, J. Chem. Phys. 121 (2004) 3405–3416.
[66] F.A. Hamprecht, A. Cohen, D.J. Tozer, N.C. Handy, Development and assessment of new exchange-correlation functionals, J. Chem. Phys. 109 (1998) 6264–6271.
[67] H.L. Schmider, A.D. Becke, Optimized density functionals from the extended G2 test set, J. Chem. Phys. 108 (1998) 9624–9631.
[68] J.M. Tao, J.P. Perdew, V.N. Staroverov, G.E. Scuseria, Climbing the density functional ladder: nonempirical meta-generalized gradient approximation designed for molecules and solids, Phys. Rev. Lett. 91 (2003) 1–4 146401.
[69] Y. Zhao, D.G. Truhlar, The M06 suite of density functionals for main group thermochemistry, thermochemical kinetics, noncovalent interactions, excited states, and transition elements: two new functionals and systematic testing of four M06-class functionals and 12 other functionals, Theor. Chem. Acc. 120 (2008) 215–241.
[70] A.D. Becke, A new mixing of Hartree-Fock and local density-functional theories, J. Chem. Phys. 98 (1993) 1372–1377.
[71] S. Grimme, Semiempirical hybrid density functional with perturbtive second-order correlation, J. Chem. Phys. 124 (2006) 1–16 034108.
[72] T. Schwabe, S. Grimme, Towards chemical accuracy for the thermodynamics of large molecules: new hybrid density functionals including non-local correlation effects, Phys. Chem. Chem. Phys. 8 (2006) 4398–4401.
[73] B.J. Lynch, D.G. Thrular, How well can hybrid density functional methods predict transition state geometries and barrier heights? J. Chem. Phys. A 105 (2001) 2936–2941.
[74] Y. Zhao, B.J. Lynch, D.G. Thrular, Development and assesment of a new hybrid density functional model for thermochemical kinetics, J. Phys. Chem. A 108 (2004) 2715–2719.
[75] J.K. Kang, C.B. Musgrave, Prediction of transition state barriers and enthalpies of reaction by a new hybrid density-functional approximation, J. Chem. Phys. 115 (2001) 11040–11051.
[76] L.A. Curtiss, P.C. Redfern, K. Raghavachari, Gaussian-4 theory, J. Chem. Phys. 126 (2007) 1–12 084108.
[77] L.A. Curtiss, P.C. Redfern, K. Raghavachari, Gaussian-4 theory using reduced order perturbation theory, J. Chem. Phys. 127 (2007) 1–8 124105.
[78] M.J. Frisch, G.W. Trucks, H.B. Schlegel, G.E. Scuseria, M.A. Robb, J.R. Cheeseman, G. Scalmani, V. Barone, B. Mennucci, G.A. Petersson, H. Nakatsuji, M. Caricato, X. Li, H.P. Hratchian, A.F. Izmaylov, J. Bloino, G. Zheng, J.L.M. Sonnenberg, Hada, M. Ehara, K. Toyota, R. Fukuda, J. Hasegawa, M. Ishida, T. Nakajima, Y. Honda, O. Kitao, H. Nakai, T. Vreven, J. A. Montgomery Jr., J. E. Peralta, F. Ogliaro, M. Bearpark, J.J. Heyd, E. Brothers, K.N. Kudin, V.N. Staroverov, R. Kobayashi, J. Normand, K. Raghavachari, A. Rendell, J.C. Burant, S.S. Iyengar, J. Tomasi, M. Cossi, N.J. Rega Millam, M. Klene, J.E. Knox, J.B. Cross, V. Bakken, C. Adamo, J. Jaramillo, R.E. Gomperts, O. Stratmann, A.J. Yazyev, R. Austin, C. Cammi, J.W. Pomelli, R. Ochterski, R.L. Martin, K. Morokuma, V.G. Zakrzewski, G.A. Voth, P. Salvador, J.J. Dannenberg, S. Dapprich, A.D. Daniels, O. Farkas, J.B. Foresman, J.V. Ortiz, J. Cioslowski, D.J. Fox, (2009) Gaussian 09. Revision D.01, Gaussian Inc., Wallingford, CT.
[79] T.J. Lee, P.R. Taylor, A diagnostic for determining the quality of single-reference electron correlation methods, Int. J. Quantum Chem. 23 (1989) 199–207.
[80] J.C. Rienstra-Kiracofe, W.D. Allen, H.F. Schaefer, The $C_2H_5 + O_2$ reaction mechanism: high-level ab initio characterizations, J. Phys. Chem. A 104 (2000) 9823–9840.
[81] J. Zheng, Y. Zhao, D.G. Truhlar, The DBH24/08 database and its use to assess electronic structure model chemistries for chemical reaction barrier heights, J. Chem. Theory Comput. 5 (2009) 808–821.
[82] S. Grimme, J. Antony, S. Ehrlich, H. Krieg, A consistent and accurate ab initio parameterization of density functional dispersion correction (DFT-D) for the 94 elements H-Pu, J. Chem. Phys. 132 (2010) 1–19 154104.
[83] Y. Zhao, N. González-García, D.G. Truhlar, Benchmark database of barrier heights for heavy atom transfer, nucleophilic substitution, association, and unimolecular reactions and its use to test theoretical methods, J. Phys. Chem. 109 (2005) 2012–2018.
[84] X. Xu, I.M. Alecu, D.G. Truhlar, How well can modern density functionals predict internuclear distances at transition state? J. Chem. Theory Comput. 7 (2011) 1667–1676.
[85] J.O. Hirschfelder, Ch.F. Curtiss, R.B. Bird, Molecular Theory of Gases and Liquids, John Wiley and Sons, Inc., New York, Chapman and Hall, Lim., London, 1954.
[86] P.J. Robinson, K.A. Holbrook, Unimolecular Reactions, Wiley-Interscience.
[87] E.V. Waage, B.S. Rabinovitch, Centrifugal effects in reaction rate theory, Chem. Rev. 70 (1970) 377–387.
[88] I. Oref, D.C. Tardy, Energy transfer in highly excited large polyatomic molecules, Chem. Rev. 90 (1990) 1407–1445.
[89] J. Troe, Theory of thermal unimolecular reactions in the fall-off range. I. Strong collision rate constants, Ber. Bunsenges. Phys. Chem. 87 (1983) 161–169.
[90] R.G. Gilbert, K. Luther, J. Troe, J. Troe, Theory of thermal unimolecular reactions in the fall-off range. II. Weak collision rate constants, Ber. Bunsenges. Phys. Chem. 87 (1983) 169–177.